Available online at www.sciencedirect.com
SCIENCE DIRECT®
Journal of Power Sources 140 (2005) 88–102
JOURNAL OF POWER SOURCES
www.elsevier.com/locate/jpowsour

A reformer performance model for fuel cell applications

S.S. Sandhu[a,*], Y.A. Saif[a], J.P. Fellner[b,*]

[a] *Department of Chemical Engineering and Materials Engineering, University of Dayton, 300 College Park, Dayton, OH 45469-0246, USA*
[b] *Air Force Research Laboratory, Propulsion Directorate, Energy Storage and Thermal Sciences, 1950 Fifth Street, Bldg. 18, WPAFB, OH 45433-7251, USA*

Received 19 July 2004; accepted 16 August 2004
Available online 1 October 2004

Abstract

A performance model for a reformer, consisting of the catalytic partial oxidation (CPO), high- and low-temperature water-gas shift (HTWGS and LTWGS), and preferential oxidation (PROX) reactors, has been formulated. The model predicts the composition and temperature of the hydrogen-rich reformed fuel-gas mixture needed for the fuel cell applications.

The mathematical model equations, based on the principles of classical thermodynamics and chemical kinetics, were implemented into a computer program. The resulting software was employed to calculate the chemical species molar flow rates and the gas mixture stream temperature for the steady-state operation of the reformer. Typical computed results, such as the gas mixture temperature at the CPO reactor exit and the profiles of the fractional conversion of carbon monoxide, temperature, and mole fractions of the chemical species as a function of the catalyst weight in the HTWGS, LTWGS, and PROX reactors, are here presented at the carbon-to-oxygen atom ratio (C/O) of 1 for the feed mixture of *n*-decane (fuel) and dry air (oxidant).

Keywords: Reformer model; Preferential oxidation; Water-gas shift reaction

1. Introduction

Due to the global enhanced concern about conserving the earth energy resources and reducing pollution, the fuel cell is a promising technology to replace the conventional internal combustion engine for power production. The ideal fuel for efficient performance is pure hydrogen in low temperature fuel cells since it simplifies system integration, maximizes system efficiency, and produces zero harmful emissions [1]. However, hydrogen is not naturally available as a fuel, but it is stored in high density in hydrocarbon fuels. Processing of hydrocarbon fuels is, therefore, necessary to extract hydrogen for stationary and mobile fuel cell applications.

Natural gas and petroleum liquids contain sulfur compounds that are harmful to a catalyst used in a fuel reformer unit to produce hydrogen. Therefore, sulfur must be removed from a sulfur-containing fuel to a level tolerable to a fuel reformer catalyst. Of the three common methods, (a) steam reforming (SR), (b) catalytic partial oxidation (CPO), (c) autothermal or oxidative steam reforming (ATR) to generate hydrogen-containing gas mixture for fuel cell applications, the CPO process is less energy consuming compared to other processes and has simpler system configuration. Catalytic partial oxidation reactions are much faster than steam reforming reactions. Therefore, smaller reactors can be realized with high throughput for hydrogen production [2]. Catalytic partial oxidation of hydrocarbon fuels (e.g. diesel, gasoline, *n*-decane, *n*-hexadecane) has been studied recently [3–5]. The results from the 5 wt.% Rh-on-γ-Al_2O_3 catalyst in a short contact time (millisecond scale) monolith reactor, have shown reaction pathways changing from combustion at low carbon to oxygen atom ratio (C/O $\ll$ 1) to syngas production around (C/O $\approx$1), and then to olefin production at higher (C/O) ratios [3]. Almost complete conversion of a fuel and oxygen are achievable with selectivity higher than 80% for syngas production for (C/O atom ratio) $\approx$1. In the

* Corresponding authors. Tel.: +1 937 229 2648; fax: +1 937 229 3433.
E-mail addresses: sarwan.sandhu@notes.udayton.edu (S.S. Sandhu), joseph.fellner@wpafb.af.mil (J.P. Fellner).

0378-7753/$ – see front matter © 2004 Elsevier B.V. All rights reserved.
doi:10.1016/j.jpowsour.2004.08.013

Nomenclature

$a_{i,e}$ activity of chemical species i in the gas–solid carbon system at the equilibrium state
$A_{F(l)}, B_{F(l)}$ first and second heat capacity coefficients of the fuel in the liquid phase
A_i, B_i, C_i, D_i constant pressure heat capacity coefficients of the chemical species in the gas phase
$A^{\alpha}_{CPO,exit}$, $B^{\alpha}_{CPO,exit}$, $C^{\alpha}_{CPO,exit}$, $D^{\alpha}_{CPO,exit}$ parameters as defined in Section 2, following Eq. (4)
$C^{\circ}_{p,i}$ constant pressure standard-state heat capacity of a gaseous chemical species i at the system temperature (J mol^{-1} K^{-1})
$d_{int,WGSR}$ internal diameter of a water-gas shift reactor (m)
D_p average diameter of particles in a packed-bed catalytic reactor (m)
f_1, f_2 functions defined in Eqs. (3c) and (3d)
G superficial mass flow velocity in a packed-bed reactor (kg m^{-2} s^{-1})
G°_i standard-state Gibbs free energy of a chemical species i at the system temperature (J (g-mol)$^{-1}$)
ΔG°_B standard-state Gibbs free energy change of the Boudouard reaction (J (g-mol)$^{-1}$)
ΔG°_{WGSR} standard-state Gibbs free energy change for the water-gas shift reaction (7) (J (g-mol)$^{-1}$)
H°_{i,T_0}, $H^{\circ}_{i,T}$ standard-state molar enthalpy of a gaseous chemical species i at a reference temperature, T_0 (e.g. T_0 = 298.15 K), and at temperature, T, respectively (J (g-mol)$^{-1}$)
ΔH°_{rxn} standard-state enthalpy of a reaction (J (g-mol)$^{-1}$)
$\Delta H^{\circ}_{rxn,CPO,T_0}$ standard-state enthalpy of the partial oxidation reaction (2) at the reference temperature, T_0 (= 298.15 K) (J (g-mol)$^{-1}$)
$\Delta H^{\circ}_{rxn,WGSR}$ standard-state enthalpy of the water-gas shift reaction (7) (J (g-mol)$^{-1}$)
$\Delta H^{\circ}_{rxn,PROX}$ standard-state enthalpy change of the CO oxidation reaction (18) occurring in the preferential oxidation (PROX) reactor (J (g-mol)$^{-1}$)
$K_{e,B}, K_{e,WGSR}$ equilibrium constants for the Boudouard and water-gas shift reactions, respectively
M_j molecular weight of a chemical species j (kg (g-mol)$^{-1}$)
$\dot{N}_j$ molar flow rate of a chemical species j in a gas mixture stream (g-mol s^{-1})
p_i partial pressure of a chemical species i in the gas-phase mixture (bar)
P total pressure (bar)
$P_{inj/vap}$ total pressure in the water injector/vaporizer unit (bar)
P° standard-state pressure (= 1 bar)
$\dot{Q}^{EXT-I}_{HTWGSR–LTWGSR}$ heat removal rate in the external intercooler (I) located between the high- and low-temperature water-gas shift reactors (J s^{-1})
$\dot{Q}^{EXT-II}_{LTWGSR–PROX}$ heat removal rate in the external intercooler (II) located between low-temperature water-gas shift and preferential oxidation reactors (J s^{-1})
$-r_{CO,HTWGSR}$ rate of CO conversion in the high-temperature water-gas shift reactor (g-mol (kg-cat.)$^{-1}$ s^{-1})
$-r_{CO,LTWGSR}$ rate of CO conversion in the low-temperature water-gas shift reactor (g-mol (kg-cat.)$^{-1}$ s^{-1})
$-r_{CO,TOF}$ turnover frequency for CO oxidation in the preferential oxidation reactor ((g-mol of CO) (g-mol of Pt atoms)$^{-1}$ s^{-1})
R gas constant (8.314 J g-mol^{-1} K^{-1})
T, T_0 temperature, the reference state temperature (e.g., T_0 = 298.15 K), respectively (K)
$T_{nbpt,F}$ normal boiling point of a liquid fuel (F) (K)
U overall heat transfer coefficient (J m^{-2} K^{-1} s^{-1})
$V_{W(l)}$ molar volume of the liquid water (m^3 g-mol^{-1})
W weight of a catalyst in a catalytic reactor (kg)
X_{CO}, $X_{CO,eq}$ actual and equilibrium fractional conversion of CO, respectively
y_i mole fraction of a chemical species in the gas phase mixture

Greek letters
α_j ratio of molar flow rate of a chemical species j to the molar flow rate of CO
β coefficient of expansion of liquid water = 638.6 $\times$ 10^{-6} K^{-1} at 100 °C
ν_i stoichiometric number of a chemical species in a chemical reaction
ϕ_b void fraction of the bed in a catalytic reactor
ρ_b bulk density of the catalyst in a packed-bed reactor (kg m$_b^{-3}$)
μ_i viscosity of a pure component i at the gas mixture temperature and pressure conditions (Pa s (= kg m^{-1} s^{-1}))
μ_{mix} viscosity of a gas-phase mixture (Pa s)
ϕ_{ij} a dimensionless quantity defined in Eq. (15c)

reformer modeling work presented in this paper, partial oxidation of *n*-decane on the Rh-on-γ-Al_2O_3 catalyst is assumed to take place. It is mentioned here that at the time of completion of this work, the chemical kinetics rate law equation for the partial oxidation of *n*-decane on this catalyst was not available for its application in the performance model presented in the next section.

The required degree of processing of the hydrogen-rich reformate from a catalytic partial oxidation reactor, e.g. Rh-on-γ-Al_2O_3 catalytic reactor, is an issue related to the type of a fuel cell. High temperature fuel cells, such as solid oxide and molten carbonate fuel cells, can directly use the reformate from a partial oxidation reactor. The requirement on the CO concentration in the fuel feed to the platinum anode of the phosphoric acid fuel cell (PAFC) is 0.25–0.5 mol% of CO. The CO tolerance for the low temperature proton exchange membrane fuel cell (PEMFC) is even lower; about 10 ppm. Presence of significant amount of CO in the fuel feed to the anode side of the low temperature fuel cells (PAFC and PEMFC) increases the anode overpotential; consequently, resulting in the reduction of the cell operational voltage and the cell electric power production. The high- and low-temperature stages of the catalytic CO conversion by its reaction with steam via shift reaction are adequate to decrease the carbon monoxide content in the reformate from a catalytic partial oxidation reactor to meet the requirement of the PAFC. Carbon monoxide removal is required after the shift reactors for PEM fuel cells by a method, such as the selective or preferential oxidation reaction. A small amount of air (typically about 2 mol%) [6] is added to the fuel stream exiting from a low-temperature, catalytic shift reactor; which then passes over a precious metal catalyst, such as the Pt-on-Al_2O_3 catalyst. This catalyst preferentially adsorbs CO, rather than H_2. Carbon monoxide, in the chemisorbed state on the catalytic active sites, reacts with the oxygen of the added air for its conversion to CO_2.

The catalytic carbon monoxide conversion, via the water-gas shift reaction ($CO\,(g) + H_2O\,(g) \Leftrightarrow H_2\,(g) + CO_2\,(g)$), is believed to take place by only two possible mechanisms. In the associative mechanism, the reactants are chemisorbed on the active sites followed by decomposition to the product species. According to the second, regenerative mechanism, the cyclic reduction–oxidation of the catalytic material leads to the formation of the product species. Both mechanisms are supported for the LTWGS catalysts; whereas the regenerative mechanism is supported for the HTWGS catalysts [7,8].

Steam to carbon monoxide molar ratio has a critical impact on the water-gas shift reaction. For the catalytic HTWGSR (e.g. Fe_3O_4 on Cr_2O_3) operation under low H_2O/CO molar ratio, formation of metallic iron is possible. Consequently, methanation, carbon deposition, and Fischer–Tropsch process can occur [7]. Copper-based catalysts (e.g. Cu-on-ZnO/Al_2O_3) for the LTWGSR have no tendency to catalyze the Fisher–Tropsch reactions and have very low activity for breaking C–O or forming C–C bond. Therefore, coke formation or carbon deposition on Cu-based LTWGSR catalysts is not a serious problem [9]. Use of a membrane, with simultaneous hydrogen separation coupled with WGSR, results in the enhancement of CO conversion when the H_2O-to-CO molar ratio is low. In comparison with the industrial HTWGS and LTWGS catalysts, the experimental results have shown that Pt-on-ZrO_2 has a potential for WGSR under low H_2O-to-CO molar ratio [10]. Research has been in progress to explore other effective catalysts for WGSR. Non-precious metals, such as Ni and Cu on cerium oxide, have shown higher activity than the conventional LTWGSR catalyst (Cu-on-Al_2O_3), for example, at high temperatures [11,12]; whereas precious metals, such as platinum group metals on cerium oxides, have shown activity in a wide temperature range [13]. Nano-scale crystals of cerium oxides with precious and non-precious metals enhance the WGSR rate. The promotion effect is attributed to the oxygen storage capacity of the oxides, when they reversibly exchange oxygen ions in the CO oxidation reaction [14,15]. When noble metals are used with cerium oxide, the WGS reactors can be operated at higher temperatures that are favorable to the kinetics. Thus, the disadvantages of the conventional WGS catalysts can be eliminated. However, currently, there are no kinetic rate law expressions, describing the WGSR on these catalysts, available.

There have been extensive efforts to find effective and selective catalysts for preferential oxidation of CO in the hydrogen-rich gas mixtures [16,17]. The relevant information on the catalytic preferential oxidation of CO over the hydrogen oxidation reaction is found in [18,19,21]. It has been found that the CO oxidation on Pt-on-Al_2O_3 catalyst increases with an increase in the reaction temperature to a maximum value, then decreases with a similar trend of the CO oxidation selectivity. This behavior is explained as follows. Carbon monoxide inhibits adsorption of H_2 at temperatures below 200 °C. At temperatures higher than 200 °C, the CO adsorption is retarded, whereas H_2 adsorption is enhanced. This results in lowering of the catalyst CO oxidation selectivity relative to hydrogen oxidation.

It has been shown that CO oxidation is a function of temperature, gas mixture composition, total gas mixture flow rate, and catalyst loading; whereas the CO oxidation selectivity is dependent only on the reactant feed gas composition and temperature. Methanation of CO and CO_2, water-gas and reverse water-gas shift reactions can possibly proceed on the Pt-on-Al_2O_3 catalyst. However, these reactions occur insignificantly in the typical CO selective temperature range 150–250 °C [20,21]; a temperature range of interest for the modeling work reported in this paper.

The fuel reformer performance model reported here is a preliminary attempt to quantitatively simulate a fuel processor to supply hydrogen-rich fuel gas mixture to a fuel cell stack operating at a relatively low temperature (e.g. solid polymer electrolyte phosphoric acid fuel cell stack). Fig. 1 shows the flow diagram of the process units of the fuel reformer. A liquid fuel (for example, *n*-decane) is vaporized and heated/mixed with air in a heater–vaporizer unit. The gas mixture leaving the heater–vaporizer unit is fed to the monolith, Rh-on-γ-Al_2O_3, catalytic partial oxidation microreactor. Partial oxidation of the fuel, *n*-decane, on the Rh-on-γ-Al_2O_3 catalyst is so fast that the conversion of *n*-decane is 100% [4] at the carbon-to-oxygen atom ratio of 1. To avoid sintering of the HTWGSR catalyst, Fe_3O_4-on-Cr_2O_3, temperature of gas exiting from the CPO reactor is decreased to an acceptable level (suitable HTWGSR operational temper-

ature range: 320–400 °C [22]). This requirement is achieved by water injection, directly, into the hot gas stream exiting from the CPO reactor. Water is also needed for the CO conversion via water-gas shift reaction. The needed water may be supplied from the cathode side of a fuel cell stack being fueled by the reformer. An external inter-cooler (EXT-I) is necessary between the HTWGSR and LTWGSR to prevent sintering of the LTWGSR catalyst, Cu-on-ZnO/Al_2O_3 (the operational temperature range: 120–250 °C) [23]. The gas mixture stream leaving the LTWGSR is cooled in the second external intercooler (EXT-II) before it enters the preferential oxidation (PROX) reactor. A small amount of air (about 2 mol%) is also added to the gas mixture stream, being cooled in the inter-cooler (EXT-II), for the preferential oxidation of CO on the Pt-on-Al_2O_3 catalyst; with the operational temperature range: 150–350 °C [21]. The product gas mixture from the preferential oxidation reactor may be fed directly to a fuel cell stack, further treated for obtaining pure hydrogen (if needed) or stored in cylinders after cooling for its later use.

2. Preliminary reformer performance mathematical model

The first unit shown in the sketch of the fuel cell reformer in Fig. 1 is the fuel vaporizer–mixer–heater. A liquid hydrocarbon fuel, *n*-decane, is injected, vaporized and mixed with dry air. The fuel/air mixer is heated to a required inlet temperature of the Rh-on-alumina catalytic partial oxidation (CPO) reactor. By the use of the first-law of thermodynamics, with the assumptions of negligible potential and kinetic energy changes and ideal gas behavior, and no shaft work exchange between the system (i.e. vaporizer–mixer–heater unit) and surroundings, the following equation for the required rate of heat supply to the vaporizer–mixer–heater unit was derived:

$$\dot{Q}_{\text{heat/vap}} = \dot{N}_{\text{F,in}}\left[R\left[A_{\text{F(g)}}(T_{\text{CPO,in}} - T_{\text{nbpt,F}}) + \frac{B_{\text{F(g)}}(T^2_{\text{CPO,in}} - T^2_{\text{nbpt,F}})}{2} + \frac{C_{\text{F(g)}}(T^3_{\text{CPO,in}} - T^3_{\text{nbpt,F}})}{3} + \frac{D_{\text{F(g)}}(T^4_{\text{CPO,in}} - T^4_{\text{nbpt,F}})}{4}\right]\Delta H^{\circ}_{\text{vap,F},T_{\text{nbpt}}} + \left[A_{\text{F(l)}}(T_{\text{nbpt,F}} - T_{\text{F(l),in}}) + \frac{B_{\text{F(l)}}(T^2_{\text{nbpt,F}} - T^2_{\text{F(l),in}})}{2}\right]\right] + \dot{N}_{\text{air,CPO,in}}\left[R\left[A_{\text{air}}(T_{\text{CPO,in}} - T_{\text{air,in}}) + \frac{B_{\text{air}}(T^2_{\text{CPO,in}} - T^2_{\text{air,in}})}{2} + \frac{C_{\text{air}}(T^3_{\text{CPO,in}} - T^3_{\text{air,in}})}{3} - D_{\text{air}}\left(\frac{1}{T_{\text{CPO,in}}} - \frac{1}{T_{\text{air,in}}}\right)\right]\right] \quad (1)$$

The first term on the right-hand side of Eq. (1) represents the amount of heat needed to vaporize and heat a liquid fuel, such as *n*-decane, to a required inlet temperature of the CPO reactor. The second term on the right-hand side represents the amount of heat needed to heat the entering air to

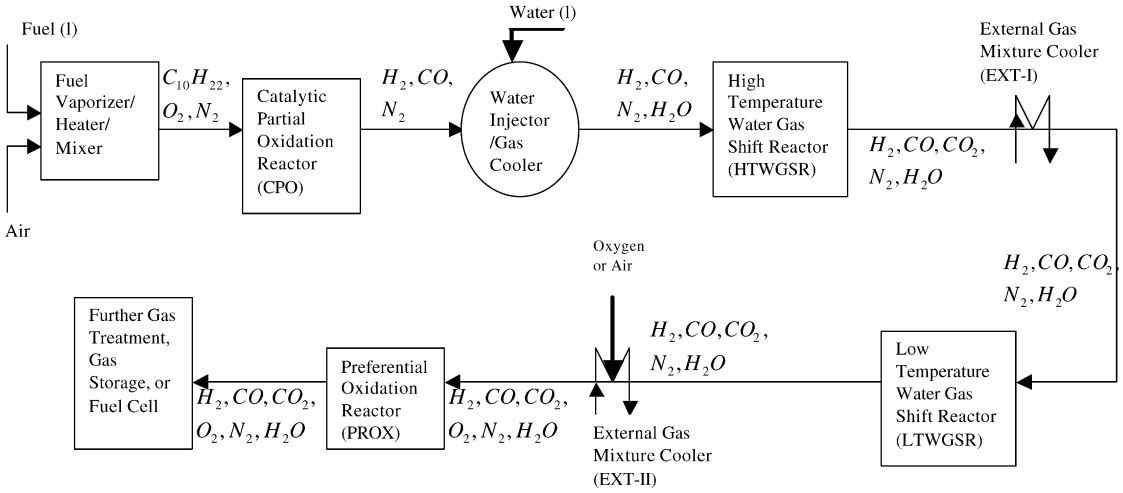

Fig. 1. Schematic diagram of a reformer to produce fuel for a fuel cell.

the CPO reactor required inlet temperature. The fuel used in our modeling/numerical simulation is *n*-decane. *n*-Decane in gas phase reacts with oxygen of the oxidant, air, according to the following partial oxidation reaction stoichiometric equation:

$$C_{10}H_{22}\,(g) + 5O_2\,(g) \rightarrow 10CO\,(g) + 11H_2\,(g) \quad (2)$$

Experimental work [3] has shown that the fuel and oxygen are almost completely consumed in the Rh-on-Al_2O_3 catalytic partial oxidation reactor at the carbon-to-oxygen atom ratio, C/O, of 1. During the period of the modeling study reported here the kinetic rate law equation for the partial oxidation reaction (2) was, unfortunately, not available [3,25]. Therefore, the assumption of complete conversion of fuel (*n*-decane) to syngas production was employed in the modeling work presented here. By the application of the first-law of thermodynamics, with the assumptions of negligible kinetic and potential energy changes, and idea-gas behavior; no shaft work exchange between the CPO reactor system and its surroundings, and under adiabatic and steady-state conditions, the following mathematical equation (3) was obtained to calculate the exit temperature of the gas mixture leaving the CPO reactor. In the formulation of Eq. (3), the air feed was assumed to be at the stoichiometric level corresponding to the carbon-to-oxygen atom ratio, C/O, of 1 in the reaction stoichiometric equation (2):

$$\tau_{CPO,exit} = 1 + \left[\frac{-\Delta H^{\circ}_{rxn,CPO,T_0} + (\tau_{CPO,in} - 1) f_1}{f_2}\right] \quad (3)$$

where

$$\tau_{CPO,in} = \left(\frac{T_{CPO,in}}{T_0}\right) \quad (3a)$$

$$\tau_{CPO,exit} = \left(\frac{T_{CPO,exit}}{T_0}\right) \quad (3b)$$

$$f_1 = R\left[\{T_0(A_F + (5A_{O_2} + 18.81A_{N_2}))\} + T_0^2(\tau_{CPO,in} + 1)\left(\frac{B_F + (5B_{O_2} + 18.81B_{N_2})}{2}\right) + T_0^3(\tau_{CPO,in}^2 + \tau_{CPO,in} + 1)\left\{\frac{C_F + (5C_{O_2} + 18.81C_{N_2})}{3}\right\} + (\tau_{CPO,in}^2 + 1)(\tau_{CPO,in} + 1) \times \left(\frac{T_0^4}{4}\right) D_F + \frac{5D_{O_2} + 18.81D_{N_2}}{T_0\tau_{CPO,in}}\right] \quad (3c)$$

$$f_2 = R\left[T_0(10A_{CO} + 11A_{H_2} + 18.81A_{N_2}) + T_0^2(\tau_{CPO,exit} + 1)\left(\frac{10B_{CO} + 11B_{H_2} + 18.81B_{N_2}}{2}\right) + T_0^3(\tau_{CPO,exit}^2 + \tau_{CPO,exit} + 1)\left(\frac{10C_{CO} + 11C_{H_2} + 18.81C_{N_2}}{3}\right) + \left(\frac{10D_{CO} + 11D_{H_2} + 18.81D_{N_2}}{T_0\tau_{CPO,exit}}\right)\right] \quad (3d)$$

The Newton–Raphson method was used to solve the nonlinear algebraic equation (3) for $\tau_{CPO,exit}$, and hence, the hot gas stream temperature at the CPO reactor exit, $T_{CPO,exit}$.

The hot gas mixture leaving the CPO reactor is cooled in the water injector/cooler unit shown in Fig. 1, by the direct injection of liquid water into the hot gas stream for efficient vaporization of liquid water and cooling of the hot gas stream to a desired inlet temperature of the HTWGSR for the catalyst sintering-free operation of the reactor. The injected water in the liquid phase, not only, meets the gas stream cooling requirement; but also, is used to satisfy the amount of water needed to convert CO to CO_2 in the high- and low-temperature water-gas shift reactors. Eq. (4) was derived to calculate the required amount of liquid water by the application of first-law of thermodynamics, with the assumptions of the idea gas mixture behavior and negligible kinetic and potential energy changes, with no shaft work exchange between the system (water injector/cooler) and its surroundings at the steady-state, adiabatic operating conditions:

$$\alpha_{W,inj} = \frac{R(\tau_{CPO,HTWGSR} - 1)[A^{\alpha}_{CPO,exit}T_{HTWGSR,in} + B^{\alpha}_{CPO,exit}T^2_{HTWGSR,in}(\tau_{CPO,HTWGSR} + 1)/2 + C^{\alpha}_{CPO,exit}T^3_{HTWGSR,in}(\tau^2_{CPO,HTWGSR} + \tau_{CPO,HTWGSR} + 1)/3 + D^{\alpha}_{CPO,exit}/T_{HTWGSR,in}\tau_{CPO,HTWGSR}]}{[(1 - \beta T_{W(l),inj})V_{W(l)}(P_{inj/vap} - P_{W(l),inj}) + \Delta H^{lv}_{H_2O,Tw(l),inj} + R(\tau_{HTWGSR,W(l),inj} - 1) \times [A_{H_2O(g)}T_{W(l),inj} + B_{H_2O(g)}T^2_{W(l),inj}(\tau_{HTWGSR,W(l),inj} + 1)/2 + C_{H_2O(g)}T^3_{W(l),inj}(\tau^2_{HTWGSR,W(l),inj} + \tau_{HTWGSR,W(l),inj} + 1)/3 + D_{H_2O(g)}/T_{W(l),inj}\tau_{HTWGSR,W(l),inj}]]} \quad (4)$$

where

$$\alpha_{\mathrm{W,inj}} = \frac{\dot{N}_{\mathrm{W,inj}}}{\dot{N}_{\mathrm{CO,CPO,exit}}},$$

$$\alpha_{j,\mathrm{CPO,exit}} = \frac{\dot{N}_{j,\mathrm{CPO,exit}}}{\dot{N}_{\mathrm{CO,CPO,exit}}},$$

$$\tau_{\mathrm{CPO,HTWGSR}} = \frac{T_{\mathrm{CPO,exit}}}{T_{\mathrm{HTWGSR,in}}},$$

$$\tau_{\mathrm{HTWGSR,W(l),inj}} = \frac{T_{\mathrm{HTWGSR,in}}}{T_{\mathrm{W(l),inj}}},$$

$$A^{\alpha}_{\mathrm{CPO,exit}} = \sum_j \alpha_{j,\mathrm{CPO,exit}} A_j,$$

$$B^{\alpha}_{\mathrm{CPO,exit}} = \sum_j \alpha_{j,\mathrm{CPO,exit}} B_j,$$

$$C^{\alpha}_{\mathrm{CPO,exit}} = \sum_j \alpha_{j,\mathrm{CPO,exit}} C_j,$$

$$D^{\alpha}_{\mathrm{CPO,exit}} = \sum_j \alpha_{j,\mathrm{CPO,exit}} D_j$$

The model equations for the high- and low-temperature water-gas shift reactors are identical except for the carbon monoxide rate law equation for its consumption. It is here assumed that the HTWGS and LTWGS packed-bed catalytic reactors have plug flow. The mole balance on CO, over a spatial element in the packed-bed reactor, was applied, under the steady-state condition, to obtain

$$\frac{\mathrm{d}X_{\mathrm{CO}}}{\mathrm{d}W} = \frac{-r_{\mathrm{CO,HTWGSR}}}{\dot{N}_{\mathrm{CO,HTWGSR,in}}} \tag{5}$$

$$\frac{\mathrm{d}X_{\mathrm{CO}}}{\mathrm{d}W} = \frac{-r_{\mathrm{CO,LTWGSR}}}{\dot{N}_{\mathrm{CO,LTWGSR,in}}} \tag{5a}$$

The rate of the CO disappearance per unit mass of the Fe_3O_4–Cr_2O_3 (90–95% Fe_3O_4, 5–10% Cr_2O_3) catalyst [22] in the HTWGSR is given by

$$-r_{\mathrm{CO,HTWGSR}} = 3.428 \times 10^9 \exp\left(\frac{-11426.51}{T}\right) c_{\mathrm{CO}}^{1.1} c_{\mathrm{H_2O}}^{0.5} (1-\zeta) \tag{6}$$

where the reversibility factor, ζ, for the water-gas shift reaction (WGSR) is given by

$$\zeta = \frac{P_{\mathrm{CO_2}} P_{\mathrm{H_2}} / P_{\mathrm{CO}} P_{\mathrm{H_2O}}}{K_{\mathrm{e,WGSR}}} \tag{6a}$$

The equilibrium constant, $K_{\mathrm{e,WGSR}}$, for the water-gas shift reaction

$$\mathrm{CO(g)} + \mathrm{H_2O(g)} \Leftrightarrow \mathrm{H_2(g)} + \mathrm{CO_2(g)} \tag{7}$$

is given by

$$K_{\mathrm{e,WGSR}} = exp\left(\frac{-\Delta G^{\circ}_{\mathrm{WGSR}}}{RT}\right) \tag{7a}$$

$$\Delta G^{\circ}_{\mathrm{WGSR}} = \sum_i v_i G^{\circ}_i \quad (i = \mathrm{CO, H_2, H_2O, CO_2}) \tag{7b}$$

where $\nu_{\mathrm{CO}} = -1$, $\nu_{\mathrm{CO_2}} = 1$, $\nu_{\mathrm{H_2O}} = -1$, $\nu_{\mathrm{H_2}} = 1$.

The rate of CO disappearance per unit mass of the $Cu/ZnO/Al_2O_3$ (Cu/Zn g-atom ratio = 2) catalyst [23] in the LTWGSR is given by

$$-r_{\mathrm{CO,LTWGSR}} = 8.22 \times 10^4 \, exp\left(\frac{-5701.23}{T}\right) p_{\mathrm{CO}} p_{\mathrm{H_2O}} (1-\zeta) \tag{8}$$

Thermal energy balance applied over a spatial element in a catalytic bed water-gas shift reactor, under the steady-state conditions, leads to

$$\frac{\mathrm{d}T}{\mathrm{d}W} = \frac{(-\Delta H^{\circ}_{\mathrm{rxn}})(-r_{\mathrm{CO}}) + U(T_{\mathrm{surr}} - T)(4/\rho_{\mathrm{b}} d_{int,\mathrm{WGSR}})}{\sum_i \dot{N}_i C^{\circ}_{p,i}} \tag{9}$$

where

$$\Delta H^{\circ}_{\mathrm{rxn}} = \sum_i v_i H^{\circ}_i \quad (i = \mathrm{CO, H_2, H_2O, CO_2}) \tag{9a}$$

U is the overall heat transfer coefficient for heat exchange between the WGSR bed and its surroundings.

Under the adiabatic condition (i.e. U = 0.0), Eq. (9) becomes

$$\frac{\mathrm{d}T}{\mathrm{d}W} = \frac{(-\Delta H^{\circ}_{\mathrm{rxn}})(-r_{\mathrm{CO}})}{\sum_i \dot{N}_i C^{\circ}_{p,i}} \tag{10}$$

Eq. (10) predicts the gas-phase temperature as a function of the catalyst weight in a water-gas shift reactor bed under the steady-state, adiabatic condition. The enthalpy or heat of the water-gas shift reaction, $\Delta H^{\circ}_{\mathrm{rxn,WGSR}}$, is given by the following derived equation:

$$\Delta H^{\circ}_{\mathrm{rxn,WGSR}} = -49222.158 + 15.464T - 0.002245T^2 + \frac{9.6775 \times 10^5}{T} \tag{11}$$

It is noted here that the differential equations (5) and (10), should be solved simultaneously to calculate the CO actual conversion, X_{CO}, and the bed gas temperature, T, as a function of the reactor bed catalyst weight. Locally, the gas phase and the catalytic particles in the reactor bed are assumed to be in thermal equilibrium. Furthermore, gradients of temperature and chemical species concentration in the radial direction in the tubular reactor are assumed to be zero.

The following expression for the equilibrium CO conversion, $X_{\mathrm{CO,eq}}$, via the water-gas shift reaction, was derived, based on the equilibrium thermodynamic fundamentals, to

compare the local actual and equilibrium CO conversion values in a catalytic water-gas shift reactor:

$$X_{CO,eq} = \frac{(1+\alpha_{H_2O})K_{e,WGSR} + (\alpha_{CO_2}+\alpha_{H_2}) \pm \sqrt{[(1+\alpha_{H_2O})K_{e,WGSR} + (\alpha_{CO_2}+\alpha_{H_2})]^2 - 4(K_e-1)(K_{e,WGSR}\alpha_{H_2O} - \alpha_{CO_2}\alpha_{H_2})}}{2(K_{e,WGSR}-1)} \quad (12)$$

where

$$\alpha_{H_2O} = \frac{\dot{N}_{H_2O,WGSR,in}}{\dot{N}_{CO,WGSR,in}}, \qquad \alpha_{CO_2} = \frac{\dot{N}_{CO_2,WGSR,in}}{\dot{N}_{CO,WGSR,in}},$$

$$\alpha_{H_2} = \frac{\dot{N}_{H_2,WGSR,in}}{\dot{N}_{CO,WGSR,in}}, \qquad \alpha_{CO} = \frac{\dot{N}_{CO,WGSR,in}}{\dot{N}_{CO,WGSR,in}} = 1$$

Of the two values of $X_{CO,eq}$ provided by Eq. (12), only the positive number value ≤ 1.0 is the acceptable one. The derived equilibrium criterion for the solid carbon formation/deposition on the catalyst in the high- or low-temperature water-gas shift reactor, via the Boudouard reaction (13) is:

$$2CO\,(g) \Leftrightarrow CO_2\,(g) + C\,(s) \quad (13)$$

At the gas mixture equilibrium state with respect to the Boudouard reaction,

$$K_{e,B} = \prod_i a_{i,e}^{\nu_i} = exp\left(\frac{-\Delta G_B^\circ}{RT}\right)$$

$$(i = CO\,(g), CO_2\,(g), C\,(s)),$$

$$\nu_{CO,B} = -2,\ \nu_{CO_2,B} = 1,\ \nu_{C,B} = 1 \quad (14)$$

$$\Delta G_B^\circ = \sum_i \nu_{i,B} G_i^\circ \quad (14a)$$

The activity of solid carbon is $a_{C(s)} = 1$ and the activity of gaseous species in the ideal gas-phase mixture at a pressure, such as 1 bar, is given by

$$a_{i,e} = \frac{y_i P}{P^\circ} \quad (i = CO, CO_2) \quad (14b)$$

Substitution for $a_{i,e}$ from Eq. (14b) into Eq. (14), on simplification, leads to:

$$\left[\frac{y_{CO_2}}{y_{CO}^2}\right]_{eq} = K_{eq}\left(\frac{P}{P^\circ}\right) \quad (14c)$$

If the actual value of $[y_{CO_2}/y_{CO}^2]_{actual}$ is greater than $[y_{CO_2}/y_{CO}^2]_{eq}$, there is a possibility of a solid carbon formation/deposition on the catalyst in a water-gas shift reactor according to the Boudouard reaction [6,26]. If $[y_{CO_2}/y_{CO}^2]_{actual}$ is less than $[y_{CO_2}/y_{CO}^2]_{eq}$, no solid carbon presence is predicted.

Total pressure drop can occur along the length of a water-gas shift reactor, predominantly, due to the presence of catalytic particles in the reactor bed. The well-known Ergun equation [27] can be used to determine the total pressure as a function of the catalyst weight, W, in the reactor:

$$\frac{dP}{dW} = -\left(\frac{4}{\pi d_{int,WGSR}^2 \rho_b}\right)\frac{G}{D_p \rho_{in}}\frac{P_{in}}{P}\frac{T}{T_{in}}\frac{1-\phi_b}{\phi_b^3} \times \left[\frac{150\mu(1-\phi_b)}{D_p} + 1.75G\right] \quad (15)$$

For the isothermal operation of a water-gas shift reactor, with negligible effect of pressure and composition on the gas mixture viscosity; Eq. (15) can be integrated to obtain

$$P = \left[P_{in}^2 - \left(\frac{8}{\pi d_{int}^2 \rho_b}\right)\left(\frac{G P_{in}}{\rho_{in} D_p}\right)\left(\frac{1-\phi_b}{\phi_b^3}\right)\left(\frac{150\mu(1-\phi_b)}{D_p} - 1.75G\right)W\right]^{0.5} \quad (15a)$$

The gas mixture viscosity, μ_{mix}, if not provided, can be calculated from the following equation [28]:

$$\mu_{mix} = \sum_{i=1}^{i=N}\left[\frac{y_i\mu_i}{\sum_{j=1}^{j=N} y_j \varphi_{ij}}\right] \quad (15b)$$

where

$$\varphi_{ij} = \frac{1}{\sqrt{8}}\left(1+\frac{M_i}{M_j}\right)^{-1/2}\left(1+\left(\frac{\mu_i}{\mu_j}\right)^{1/2}\left(\frac{M_j}{M_i}\right)^{1/4}\right)^2 \quad (15c)$$

It should be noted that a pure component viscosity, μ_i, is at the gas mixture temperature and pressure conditions. Furthermore, it has been shown that the semiempirical formula, Eq. (15b), reproduces measured values of the viscosities of the gas mixtures within an average deviation of about 2%.

External intercoolers (EXT-I and EXT-II, see Fig. 1) are needed between the HTWGS and LTWGS and between the LTWGS and PROX reactors to adjust the reactive mixture stream temperature to the desired levels prior to its entry to the LTWGS and PROX reactors. One should make it certain that the reactive gas mixture temperatures at the inlets of the LTWGS and PROX reactors are such that the temperature profiles in these reactors are within the operational temperature ranges of the catalysts in these reactors to prevent sintering of the catalyst and its activity decay. By the application of first-law of thermodynamics; with the assumptions of

negligible kinetic and potential energy changes, and ideal gas mixture behavior; and no shaft work, the following equation has been derived for the required heat removal rate in the external intercooler, EXT-I, between the HTWGS and LTWGS reactors, for the cooler steady-state operation:

$$Q^{\text{EXT-1}}_{\text{HTWGSR–LTWGSR}} = -R(\tau_{\text{HTWGSR,exit}} - 1)\left\{\left(\sum_j \dot{N}_{j,\text{HTWGSR,exit}} A_j\right) T_{\text{LTWGSR,in}} + \left(\frac{\sum_j \dot{N}_{j,\text{HTWGSR,exit}} B_j}{2}\right) \times T^2_{\text{LTWGSR,in}}(\tau_{\text{HTWGSR,exit}} + 1) + \left(\frac{\sum_j \dot{N}_{j,\text{HTWGSR,exit}} C_j}{3}\right) T^3_{\text{LTWGSR,in}}(\tau^2_{\text{HTWGSR,exit}} + \tau_{\text{HTWGSR,exit}} + 1) + \frac{\sum_j \dot{N}_j D_j}{T_{\text{LTWGSR,in}}\tau_{\text{HTWGSR,exit}}}\right\} \quad (16)$$

(j = H_2, H_2O, CO, CO_2, N_2, and O_2 if left unreacted in the CPO reactor).

where

$$\tau_{\text{HTWGSR,exit}} = \frac{T_{\text{HTWGSR,exit}}}{T_{\text{LTWGSR,in}}} \quad (16a)$$

Eq. (16) is a simple algebraic equation, the required heat removal rate in the external intercooler, EXT-I, can be calculated by simply substituting the values of the chemical species molar flow rates, exit temperature of the reactive mixture stream leaving the HTWGSR, its required temperature at the inlet of the LTWGSR, and the heat capacity coefficients for the chemical species present in the gas mixture stream.

If the gas mixture stream leaving the LTWGSR does not contain sufficient amount of oxygen to convert CO in the PROX reactor to a desired conversion level, oxygen or air is added, at a controlled rate, to the hot gas stream either prior to the external intercooler, EXT-II, or in concurrence with its cooling in the cooler. Addition of oxidant in this manner should result in the lesser required heat removal rate in the EXT-II cooler. Air may be added at its ambient temperature. The derived equation for the heat removal rate in the external intercooler, EXT-II, for its steady-state operation is:

$$Q^{\text{EXT-II}}_{\text{LTWGSR–PROX}} = \left[\sum_i^{\text{LTWGSR–exit}} \dot{N}_i H_{i,T_{\text{LTWGSR–exit}}} + \text{oxidant stream}\sum \dot{N}_{i,T_{\text{oxidant}}} H_{i,T_{\text{oxidant}}}\right] - \left[\sum_i^{\text{PROX}} \dot{N}_i H_{i,T_{\text{PROX–in}}}\right] \quad (17)$$

where

$$H_{i,T} = H^0_{i,T} = H^0_{i,T_0} + \int_{T_0}^{T} Cp_i \, \mathrm{d}T \quad (17a)$$

The first and second sum terms within the square brackets on the right-hand side of Eq. (17) are the enthalpy flow rates associated with the hot gas stream leaving the LTWGSR and the oxidant stream, respectively. The third sum term is the enthalpy flow rate associated with the stream entering the PROX reactor.

The preferential oxidation reactor is used to decrease the CO concentration in the hydrogen-containing gas stream to an acceptable level for its ultimate application in a low-temperature fuel cell stack (for example, phosphoric acid electrolyte fuel cell stack). Carbon monoxide oxidation takes place on the Pt-on-Al_2O_3 catalyst via the following reaction stoichiometric equation:

$$\text{CO (g)} + \tfrac{1}{2}\text{O}_2\text{ (g)} \Leftrightarrow \text{CO}_2\text{ (g)} \quad (18)$$

This reaction (18) is selectively accelerated relative to the hydrogen oxidation reaction on this catalyst.

$$\text{H}_2\text{ (g)} + \tfrac{1}{2}\text{O}_2\text{ (g)} \Leftrightarrow \text{H}_2\text{O (g)} \quad (18a)$$

The intrinsic chemical reaction rate law equation for CO oxidation [21] is:

$$-r_{\text{CO,TOF}} = 3.1 \times 10^8 \exp\left(\frac{-9742.6}{T}\right) p_{\text{CO}}^{-0.5} p_{\text{O}_2}^{0.81} \quad (19)$$

This rate law equation is for the Pt-on-Al_2O_3 catalyst, with 10% (by weight) of the platinum loading and 60% dispersion of platinum atoms. The above kinetic rate law equation is valid over the temperature range: 423–623 K. The plug flow type, carbon monoxide mole balance and thermal energy balance equations similar to Eqs. (5) and (10), respectively, are used to predict the CO conversion and the gas temperature as a function of the catalyst weight in the PROX reactor. Locally, thermal equilibrium between the gas and catalytic particle solid phase is assumed. The enthalpy or heat of reaction (18), $\Delta H^\circ_{\text{rxn,PROX}}$, is given below for its use in the thermal energy equation for the PROX reactor:

$$\Delta H^\circ_{\text{rxn,PROX}} = -286543.83 + 2.174T + 9.77 \times 10^{-4}T^2 + \frac{8.42 \times 10^5}{T} \quad (20)$$

3. Numerical simulation

A computer program was developed in Microsoft Visual Basic 6.0 to generate numerical data from the model performance equations [29]. The input parameters to the computer program are the inlet molar flow rates of the fuel, *n*-decane, and air; the system pressure, inlet temperature of the fuel and air to the heater–vaporizer unit, inlet temperature of the gas mixture to the catalytic partial oxidation (CPO) reactor, temperatures at the inlets of the HTWGS, LTWGS and PROX reactors, and molar flow rate ratio, O_2/CO, at the inlet of the PROX reactor. It is here mentioned that some of the reformer performance model equations presented in Section 2, for example, the solid carbon presence criterion and reactor pressure drop equations, were not in the final computer simulation stage at the time of writing of this paper. Also, the reference [24,26,29] should be cited for other parameter numerical data.

The heater–vaporizer, water injector/cooler, and external cooler EXT-I and EXT-II model equations are simple algebraic equations. The solution of these equations is straightforward. Newton–Raphson method is used to estimate the exit

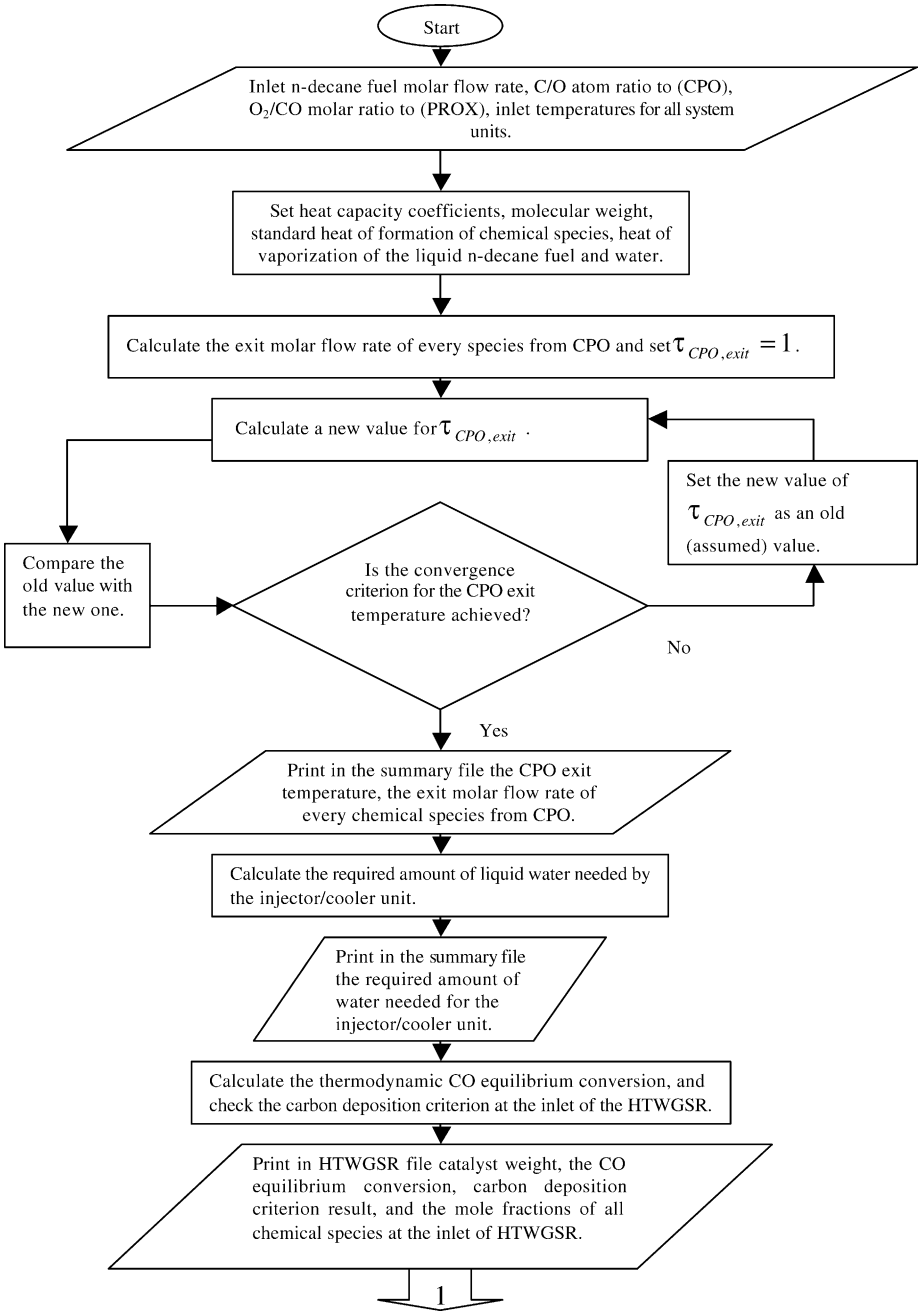

Fig. 2. Flow diagram of the program steps for the fuel reformer modeling.

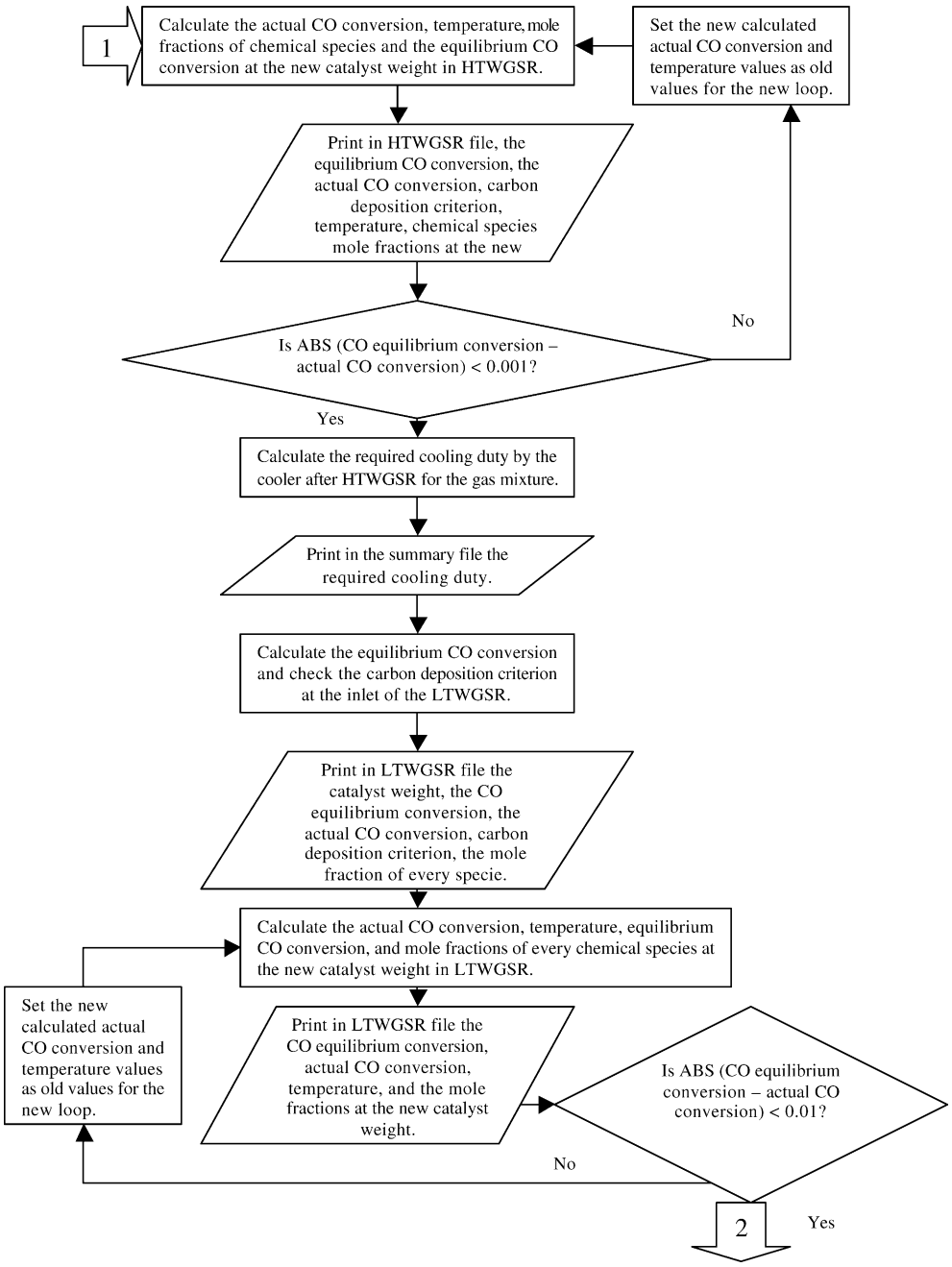

Fig. 2. (*Continued*)

temperature from the CPO reactor. The coupled CO mole balance and energy equations are solved simultaneously by the fourth-order Runge–Kutta method in the HTWGS, LTWGS, and PROX reactors. Fig. 2 shows the flowchart of the execution steps in the program.

4. Results and discussion

Fig. 3 shows the effect of the CPO reactor inlet temperature on the gas mixture temperature leaving the CPO reactor at the carbon to oxygen atom ratio of 1. The nature of the gas mixture outlet temperature versus the gas mixture inlet temperature plot is totally dependent on Eq. (3) given in Section 2. It is almost straight line over the inlet temperature range 480–520 K. Results presented in Figs. 4 and 5 correspond to the parametric conditions given in Table 1.

Fig. 4 shows the change of actual CO conversion, equilibrium CO conversion, and gas mixture temperature as a function of the catalyst weight in the HTWGSR. The gas mixture temperature increases with an increase in the catalyst weight due to the exothermic nature of the water-gas shift reaction;

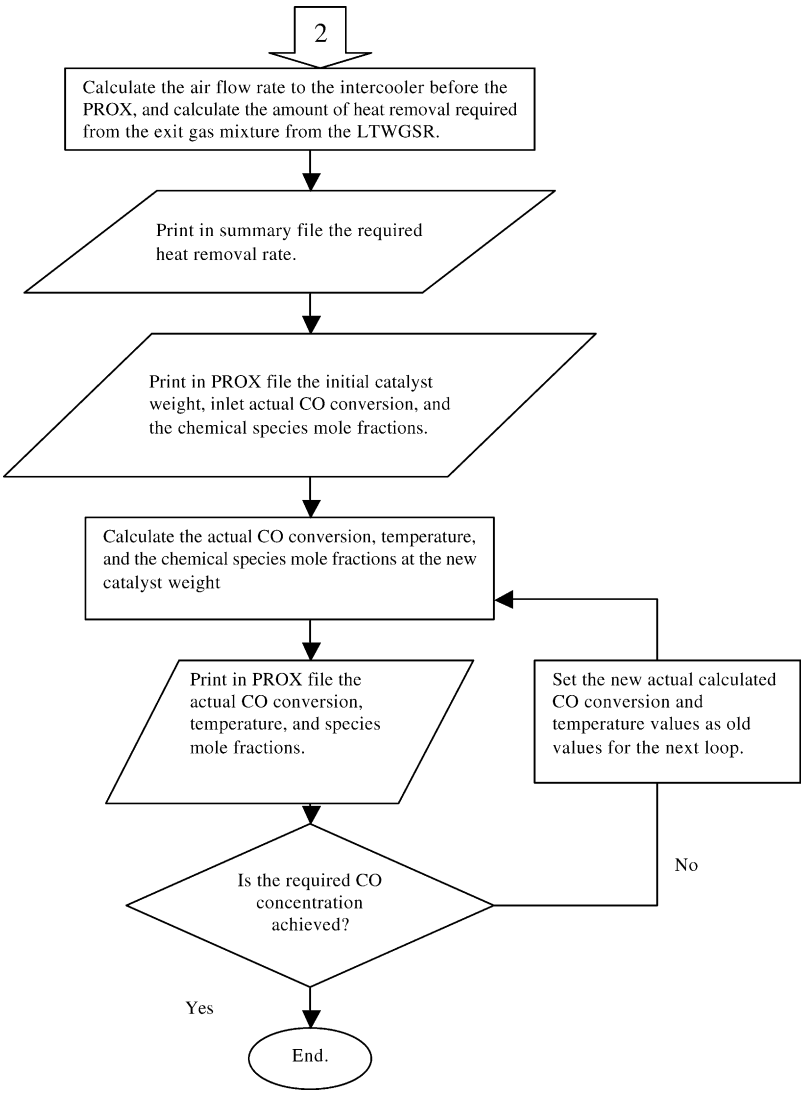

Fig. 2. (*Continued*).

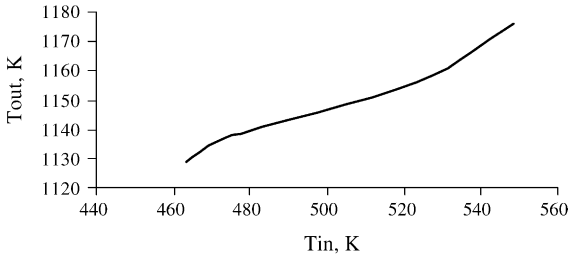

Fig. 3. The effect of the inlet temperature of the gas mixture on the exit temperature of the CPO reactor.

Table 1
Parametric data at carbon-to-oxygen atom ratio of 1

Fuel (n-$C_{10}H_{22}$) feed rate (g-mol s^{-1})	1.087×10^{-3}
Air feed rate (g-mol s^{-1})	2.5879×10^{-2}
System pressure (bar)	1.2
Fuel and air inlet temperature (°C)	25
Temperatures at the inlets of CPO, HTWGS, LTWGS and PROX reactors (°C)	250, 200, 177, 147

whereas the equilibrium CO conversion decreases and the actual CO conversion increases with the increase in catalyst weight. Since the water-gas shift reaction is reversible and the actual CO conversion is limited by the principles of equilibrium thermodynamics; the point, where the actual and equilibrium CO conversion curves meet, is the point of maximum actual CO conversion.

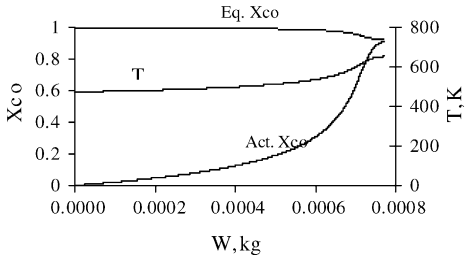

Fig. 4. Temperature, actual and equilibrium CO conversion vs. catalyst weight in the HTWGSR.

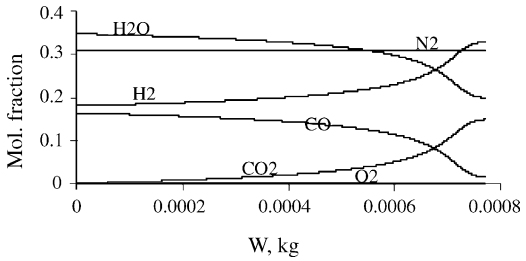

Fig. 5. Mole fraction profiles of chemical species in the gas mixture in the HTWGSR vs. the catalyst weight.

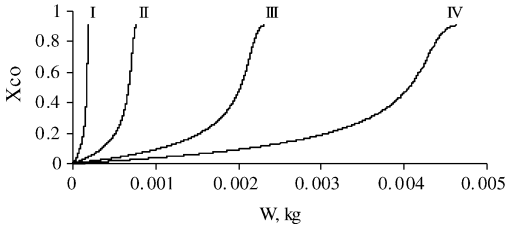

Fig. 6. The effect of total inlet molar flow rate on CO conversion in the HTWGSR.

Fig. 5 shows the species mole fraction profiles as a function of the catalyst weight in the HTWGSR. Nitrogen and oxygen (oxygen in trace amount) mole fractions are constant with respect to the catalyst weight along the reactor length; because, they are not involved in the water-gas shift reaction and the total gas mixture molar flow rate does not change due to the nature of the reaction stoichiometric equation. Mole fractions of the product species, hydrogen and carbon dioxide, increase; whereas those of the reactant species, carbon monoxide and water, decrease. Fig. 6 shows the effect of the total fuel and air molar feed rate on the actual CO conversion versus the catalyst weight profile in the HTWGSR at the carbon-to-oxygen atom ratio of 1. The total molar feed rate setting numbers I, II, III and IV correspond to the molar flow rates given in Table 2 and the other parametric data are the same as shown in Table 1.

From Fig. 6, it is apparent that a higher amount of the catalyst is needed for a higher total molar feed rate compared to that for a lower total molar feed rate to achieve the same fractional conversion of CO.

Figs. 7–9 show the plotted, computed data for the LTWGSR similar to the HTWGSR data. The explanation for these plots is exactly similar to that given above for the HTWGSR plots. However, the catalyst weight in the LTWGSR is in the order of kg whereas that is in the order of mg in the HTWGSR. This is due to the lower chemical kinetics rate affected by the lower operational temperature range that prevails in the catalytic LTWGS reactor bed. One should carefully control the temperature of the gas mixture entering the LTWGSR so that the temperature of the gas mixture leaving it is less than 260 °C to prevent sintering of the copper catalyst. Also, the copper catalysts do not have strong activity toward breaking of C–O bond; and hence, the danger of carbon formation/deposition via the Boudouard reaction is less compared to the iron-based HTWGSR catalyst [7].

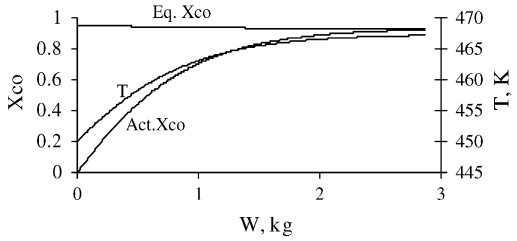

Fig. 7. Temperature, actual and equilibrium CO conversion vs. catalyst weight in the LTWGSR.

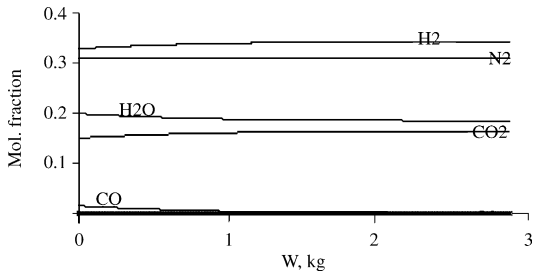

Fig. 8. Mole fraction of the chemical species vs. catalyst weight in the LTWGSR.

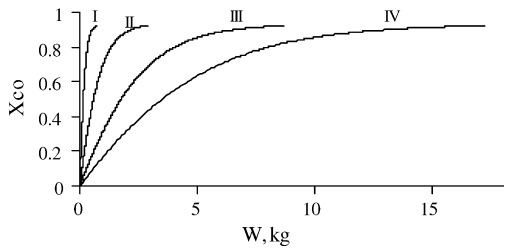

Fig. 9. Effect of the total inlet molar feed rate on the profile of the actual CO conversion vs. the catalyst weight in the LTWGSR.

The preferential oxidation (PROX) reactor results shown in Figs. 10–13 correspond to the reformer parametric feed

Table 2
Reactant feed data at the carbon-to-oxygen atom (C/O) ratio = 1

Reactant feed rate setting number	Fuel (n-$C_{10}H_{22}$) molar flow rate (g-mol s^{-1}) (A)	Air feed flow rate (g-mol s^{-1}) (B)	Total molar feed rate = A + B (g-mol s^{-1})
I	2.717E−04	6.4696E−03	6.7413E−03
II	1.087E−03	2.5879E−02	2.6966E−02
III	3.261E−03	7.7636E−02	8.0897E−02
IV	6.0E−03	14.2857E−02	14.8857E−02

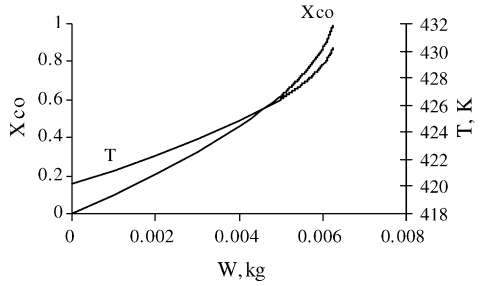

Fig. 10. CO conversion and temperature profiles vs. catalyst weight in the PROX reactor.

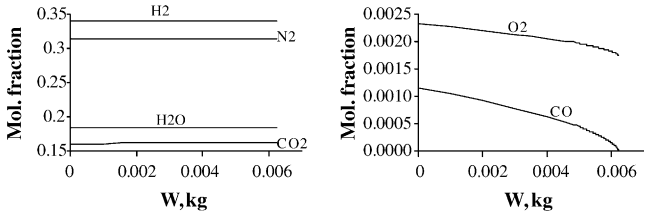

Fig. 11. Mole fraction of the chemical species vs. catalyst weight in the PROX reactor.

rate data given in Table 1. Fig. 10 shows the actual CO conversion and temperature profiles as a function of the catalyst weight in the PROX reactor for the inlet oxygen to carbon monoxide molar ratio of 2. Close to the reactor inlet, the CO conversion and the gas mixture temperature increase almost linearly as a function of the Pt-on-Al_2O_3 catalyst weight. As the CO concentration decreases with an increase in the catalyst weight, the rise in the actual CO conversion becomes relatively steep. The gas mixture temperature follows a similar trend. This observed behavior is in agreement with [30]. The CO oxidation rate has a negative order with respect to CO concentration. An increase in the bed temperature and a decrease in the CO concentration in the ppm range result in a relatively high value of the CO oxidation rate, and hence, in the actual CO conversion.

The profiles of the mole fractions of chemical species as a function of the catalyst weight in the (PROX) reactor are shown in Fig. 11. Carbon monoxide and oxygen being the reactant species, their mole fractions decrease with an increase in the catalyst weight; whereas the mole fraction of the product CO_2 increases with the catalyst weight increase. Hydrogen, nitrogen, and water species were assumed not to take part in any reaction. Therefore, their molar flow rates do not change with an increase in the catalyst. However, their mole fractions increase slightly with an increase in the catalyst weight due to the decrease in the total mixture molar flow rate associated with the occurrence of the CO oxidation reaction. Fig. 12 shows the effect of the PROX reactor inlet temperature on the actual CO conversion versus catalyst weight profile. One observes that the weight of the catalyst needed is less for a higher inlet temperature for the same actual CO conversion. However, with an increase in the bed temperature, CO desorption from the catalytic surface is enhanced. This affects the catalyst selectivity towards the CO oxidation relative to the hydrogen oxidation. At a higher temperature, the hydrogen oxidation rate increases [20,21]. Therefore, optimization of the gas mixture temperature at the PROX reactor inlet is essential to realize the enhanced catalyst selectivity to CO oxidation. The inlet oxygen-to-carbon monoxide molar ratio is an important parameter in the CO oxidation process in the preferential oxidation reactor. Fig. 13 shows the effect of the inlet oxygen-to-carbon monoxide molar ratio on the actual CO conversion versus the catalyst weight profile. From the plots, it is apparent that a lesser amount of the catalyst is needed at a higher oxygen-to-carbon monoxide molar ratio than that at a lower oxygen-to-carbon monoxide molar ratio to achieve the same actual CO fractional conversion. This suggests that the PROX reactor should be operated at a value higher than the stoichiometric value of 0.5 of the oxygen to carbon monoxide molar ratio to reduce the amount of catalyst needed. However, the selected oxygen to carbon monoxide molar ratio should be such that the hydrogen (desired fuel-cell fuel) oxidation is still insignificant relative to the CO oxida-

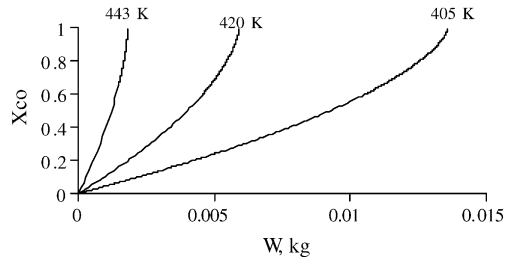

Fig. 12. Inlet gas mixture temperature effect on CO conversion in the PROX reactor.

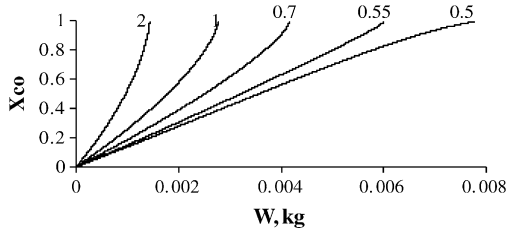

Fig. 13. Effect of the inlet molar O_2/CO ratio on CO conversion in the PROX reactor.

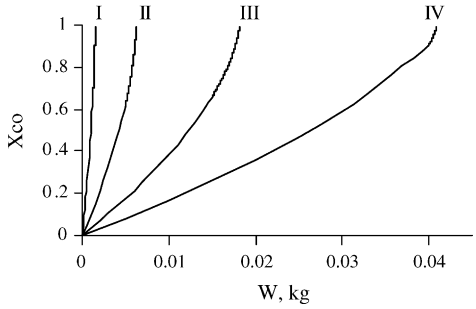

Fig. 14. Effect of total inlet molar flow rate on CO conversion in the PROX reactor.

tion process on the Pt-on-Al_2O_3 catalyst in the PROX reactor. Fig. 14 shows the effect of the total reactant molar feed rate to the reformer on the actual CO conversion versus catalyst weight profile for the four flow rates given in Table 2. It is quite obvious that a larger amount of catalyst is needed for a larger total reactant molar feed rate to the reformer for a fixed actual CO fractional conversion. This is so because the PROX reactor is then required to oxidize a larger amount of CO.

5. Conclusions

(a) A preliminary mathematical model, based on the principles of thermodynamics and chemical reaction engineering, has been developed to predict the performance of a reformer for the production of hydrogen-rich gas mixture from a hydrocarbon fuel, such as *n*-decane (here used as a model compound for the JP-10 ($C_{10}H_{16}$) fuel), for the fuel cell applications. Although the model was originally developed for the carbon-to-oxygen atom ratio of one with *n*-decane as the fuel and air as the oxidant, the model can be adapted to the non-stoichiometric feeds of a fuel and air for the partial oxidation of the fuel in the Rh-on-γ-Al_2O_3 catalytic partial oxidation reactor to produce syngas for its further treatment in the water-gas shift and preferential oxidation reactors.

(b) A computer program, based on the performance model equations, was developed and implemented to numerically simulate the performance of the fuel processor shown in Fig. 1.

(c) The relation between the predicted exit gas mixture temperature and the inlet temperature of the gas mixture entering the CPO reactor may be approximated by a linear relation.

(d) The computed performance data for the HTWGS and LTWGS reactors show similar trends. The gas mixture temperature and the actual CO conversion increase, with an increase in the catalyst weight, to their equilibrium state values. Optimization of the gas mixture temperature at the inlet of the HTWGSR as well as of the LTWGSR is important to avoid sintering of the catalyst and reduce its weight in each reactor for a desired overall actual CO conversion in these reactors. This also has the effect on the amount of water needed for injection into the water injector/gas cooler unit. One should make it certain that the amount of water injected is sufficient to convert the entire amount of CO in the gas mixture entering the HTWGSR–external cooler–LTWGSR module.

(e) The reaction rate for the CO oxidation in the PROX reactor, as predicted by the empirical equation (19), shows an interesting behavior. It changes from a low to a relatively high value as the actual CO conversion approaches unity. One may explain this in terms of the competition between carbon monoxide, hydrogen, and oxygen for their chemisorption at the catalytic active sites for the overall CO oxidation process.

6. Suggestions

(a) In the performance model presented in this paper, the assumption of complete conversion of a fuel, such as *n*-decane, and oxidant (air) at the carbon-to-oxygen atom ratio of 1 was used due to the non-availability of the chemical kinetics rate equation for the partial oxidation reaction on Rh-on-Al_2O_3 catalyst in the catalytic partial oxidation (CPO) reactor. It is suggested that first the kinetic rate law equation for the partial oxidation of a fuel, for example, *n*-decane (*n*-$C_{10}H_{22}$) or JP-10 ($C_{10}H_{16}$) be developed through experimental work. Then, this rate law equation should be incorporated into the current reformer performance model to predict the CPO reactor performance behavior as well as that of the overall reformer system for different carbon-to-oxygen atom ratios or for different fuel and air feed rates.

(b) It is suggested that a small-scale fuel reformer, based on the scheme presented in Fig. 1, be designed and built so that the experimental program can be initiated to acquire the experimental data for the improvement/validation of the reformer performance model presented here.

Acknowledgments

Financial support for this work was provided by the Air Force Research Laboratory, Wright-Patterson AFB, Ohio; under contract number: F33615-98-D2891, delivery order 17. Y.A. Saif would like to thank the Saudi Higher Education Ministry for the financial support for his graduate work at the University of Dayton.

References

[1] C. Song, Catal. Today (2002) 77.
[2] S.S. Bharadwaj, L.D. Schmidt, Fuel Proc. Tech. (1995) 42.
[3] J.J. Krummenacher, K.N. West, L. Schmidt, J. Catal. 215 (2003) 332–343.
[4] L.D. Schmidt, E.J. Klein, C.A. Leclerc, J.J. Krummenacher, K.N. West, Chem. Eng. Sci. 58 (2003) 1037–1041.
[5] E. Newson, T.B. Truoung, Int. J. Hydrogen Energy 28 (2003) 1379–1386.
[6] J. Larminie, A. Dicks, Fuel Cell Systems Explained, 2nd ed., Wiley, 2003, pp. 251–252.
[7] M.V. Twigg (Ed.), Catalyst Handbook, 2nd ed., Wolfe Press, London, 1990, pp. 282–339.
[8] C. Rhodes, G.J. Hutchings, A.M. Ward, Catal. Today 23 (1995) 43–58.
[9] M.V. Twigg, M.S. Spencer, Appl. Catal. A: General 212 (2001) 161–174.
[10] E. Xue, M. Okeeffe, J.R.H. Ross, Catal. Today 30 (1996) 107–118.
[11] Y. Li, Q. Fu, M. Flytzani-Stephanopoulos, Appl. Catal. B: Environ. 27 (2000) 179–191.
[12] S. Hilaire, X. Wang, T. Luo, R.J. Grote, J. Wagner, Appl. Catal. A: General 215 (2001) 271–278.
[13] T. Bunluesin, R.J. Grote, G.W. Graham, Appl. Catal. B: Environ. 15 (1998) 107–114.
[14] S.L. Swartz, M.M. Seabaugh, C.T. Holt, W.J. Dawson, Fuel Cells Bull. 30 (2001) 7–10.

[15] A. Holmgren, B. Anderson, D. Duprez, Appl. Catal. B: Environ. 22 (1999) 215–230.
[16] S.H. Oh, R.M. Sinkevitch, J. Catal 142 (1993) 254–262.
[17] M.L. Brown, A.W. Green, G. Cohn, H.C. Anderson, Ind. Eng. Chem. 52 (1960) 841.
[18] O. Korotkikh, R. Farrauto, Catal. Today 62 (2000) 249–254.
[19] A. Manaslip, E. Gulari, Appl. Catal. B: Environ. 37 (2002) 17–25.
[20] M.J. Kahlich, H.A. Gasteiger, R.J. Behm, J. Catal. 171 (1997) 93–105.
[21] D.H. Kim, M.S. Lim, Appl. Catal. A: General 224 (2002) 27–38.
[22] R.L. Keiski, T. Salmi, P. Niemisto, J. Ainassaari, V.J. Pohjola, Appl. Catal. A: General 137 (1996) 349–370.
[23] Y. Choi, H.G. Stenger, J. Power Sources 124 (2003) 432–439.
[24] B.E. Poling, J.M. Prausnitz, J.P. O'Connell, The Properties of Gases and Liquids, 5th ed., McGraw-Hill, 2001, p. A44.
[25] A. Naidja, C.R. Krishna, T. Butcher, D. Mahajan, Prog. Energy Combust. Sci. 29 (2003) 155–191.
[26] J.M. Smith, H.C. Van Hess, M.M. Abbot, Introduction to Chemical Engineering Thermodynamics, 6th ed., McGraw-Hill, New York, 2003, pp. 523, 657.
[27] R.B. Bird, W.E. Stewart, E.N. Lightfoot, Transport Phenomena, Wiley, 1960, 200 pp.
[28] R.B. Bird, W.E. Stewart, E.N. Lightfoot, Transport Phenomena, 2nd ed., Wiley, New York, 2002, 27 pp.
[29] Y.A. Saif, Preliminary numerical simulation of a reformer performance model for fuel cell applications, Master of Science in Chemical Engineering, Thesis, The University of Dayton, Dayton, OH, 2004.
[30] G.F. Froment, K.B. Bischoff, Chemical Reactor Analysis and Design, 2nd ed., Wiley, 1990, pp. 174, 175.